Land-atmosphere feedbacks reduce evaporative demand in a warming climate: implications at local and global scales

Yeonuk Kim[1*], Monica Garcia[2], and Mark S. Johnson[1, 3]

[1]Institute for Resources, Environment and Sustainability, University of British Columbia; Vancouver, V6T1Z4, Canada.

[2] Research Centre for the Management of Agricultural and Environmental Risks (CEIGRAM). E.T.S.I. Agronomica, Alimentaria y de Biosistemas. Universidad Politecnica de Madrid, Spain.

[3] Department of Earth, Ocean and Atmospheric Sciences, University of British Columbia; Vancouver, V6T1Z4, Canada.

Corresponding author: Yeonuk Kim (yeonuk.kim.may@gmail.com)

Key Points:

- Potential evaporation models overestimate evaporative demand for warmer future climatic conditions, leading to a hydrologic drying bias.
- To resolve this, we developed and evaluated a land-atmosphere coupled potential evaporation model to estimate future evaporative demand.
- Evaporative demand will likely increase slower than previously thought, implying land-atmosphere feedbacks moderates continental drying.

Abstract

The magnitude and extent of runoff reduction, drought intensification, and dryland expansion under climate change are unclear and contentious. A primary reason is disagreement between global circulation models and current potential evaporation (PE) models for evaporative demand under warming climatic conditions. An emerging body of research suggests that current PE models including Penman-Monteith and Priestley-Taylor may overestimate future evaporative demand. However, they are still widely used for climatic impact analysis although the underlying physical mechanisms for PE projections remain unclear. Here, we show that current PE models diverge from observed non-water-stressed evaporation, a proxy of evaporative demand, across site (>1500 flux tower site years), watershed (>10,000 watershed-years), and global (25 climate models) scales. By not incorporating land-atmosphere feedback processes, current models overestimate non-water-stressed evaporation and its driving factors for warmer and drier conditions. To resolve this, we introduce a land-atmosphere coupled PE model that accurately reproduces non-water-stressed evaporation across spatiotemporal scales. We demonstrate that terrestrial evaporative demand will increase at a similar rate to ocean evaporation, but much slower than rates suggested by current PE models. This finding suggests that land-atmosphere feedbacks moderate continental drying trends. Budyko-based runoff projections incorporating our PE model are well aligned with those from coupled climate simulations, implying that land-atmosphere feedbacks are key to improving predictions of climatic impacts on water resources. Our approach provides a simple and robust way to incorporate coupled land-atmosphere processes into water management tools.

Plain Language Summary

Water resources are supply-side constrained by precipitation, and demand-side constrained by atmospheric evaporative demand. It is important to understand how supply and demand sides of hydroclimate features change with time, particularly for projected future climatic conditions. Conventionally, a warming and drying climate system has been understood to increase atmospheric evaporative demand. However, this demand-side perspective neglects land-atmosphere feedback effects. For example, hot dry air is also an indicator of dry soil, implying that increasing demand (e.g., hot dry air) may not be met due to supply constraints (e.g., dry soil). We introduce a land-atmosphere coupled potential evaporation model to better predict evaporative demand under future climatic conditions. In evaluating the model across site, watershed, and global scales, we report a slower increase in evaporative demand in a warming climate compared to studies not incorporating land-atmosphere coupling, which is significant for water resources planning. Improved representation of evaporative demand under future climate conditions is necessary to aid in planning for climate adaptation, including agricultural water management, improvement of fire risk indices, and other critical societal informational needs.

1 Introduction

Atmospheric evaporative demand, which sets the upper limit of evaporation, is widely used as a key constraint for estimating actual evaporation and evapotranspiration, as well as runoff, crop water use, aridity, and drought (Ault, 2020; Vicente-Serrano et al., 2020). The evaporative demand exerted by the atmosphere is commonly determined as potential evaporation (PE), which is operationally understood as the evaporation rate when evaporation is not limited by soil moisture (Vicente-Serrano et al., 2020). Among various proposed PE models, Penman-Monteith and Priestley-Taylor PE are the most widely used since their underlying definitions and formulations are primarily physically-based. As such, these PE equations are widely used to predict and analyze changes in drought, aridity, and water availability in relation to a changing climate (Dai, 2013; Peter Greve et al., 2014; Marvel et al., 2019; McEvoy et al., 2020; P. C. D. Milly & Dunne, 2020; Piemontese et al., 2019; Sheffield et al., 2012; Su et al., 2018; Trenberth et al., 2013; Wang et al., 2018).

According to current PE models, PE under climate warming is projected to increase at a greater rate than precipitation over land, leading to increased aridity (Scheff & Frierson, 2014; Sherwood & Fu, 2014). Therefore, many studies have sought to explore the implications of enhanced land surface drying under climate change. However, several recent studies have demonstrated that calculations based on PE lead to overestimation of non-water-stressed evaporation for warmer and drier future climate conditions (P. C. D. Milly & Dunne, 2016; P.C.D. Milly & Dunne, 2017), resulting in overestimates of actual evapotranspiration, soil drying, and runoff reductions compared to direct projections by climate models (P. C. D. Milly & Dunne, 2016; P.C.D. Milly & Dunne, 2017; Roderick et al., 2015; Yuting Yang et al., 2019). More recently, the widely accepted dryland expansion trend under climate change (Berdugo et al., 2020; J. Huang et al., 2016; Overpeck & Udall, 2020) has been questioned (Berg & McColl, 2021; P. Greve et al., 2019; Keenan et al., 2020; Shi et al., 2021), and debate on the magnitudes of past and future trends in drought has intensified (Berg & Sheffield, 2018; Swann et al., 2016; Tomas-Burguera et al., 2020; Y. Yang et al., 2020). These scientific debates originate to a large extent as a result of PE overestimation (Berg & Sheffield, 2018; Vicente-Serrano et al., 2020). Therefore, there is an urgent need to re-evaluate PE to correctly understand and predict climatic impacts on water resources.

Current physically-based PE models assume saturated or near saturated surface conditions, and these land surface conditions are assumed to be stationary. Based on this assumption, the Clausius-Clapeyron relationship (i.e., the relationship between temperature and saturation vapour pressure) can be introduced, resulting in a positive, exponential relationship between temperature and PE. As a result, Priestley-Taylor PE, which is based on the equilibrium evaporation concept, is largely controlled by temperature. While Penman-Monteith PE also scales with temperature, a decrease in atmospheric relative humidity also results in increased values for the Penman-Monteith PE due to the increased vertical gradient of relative humidity from the functionally saturated land surface relative to the overlying atmosphere. Consequently, warmer and drier atmospheric future conditions result in substantially increased PE computed using current PE models.

However, the stationary land surface assumptions in PE models are not necessarily robust. For instance, elevated atmospheric CO_2 concentrations can increase the surface resistance, an empirical parameter in the Penman-Monteith model (Swann et al., 2016; Yuting Yang et al., 2019; Y. Yang et al., 2020). To resolve the CO_2 fertilization effect, Yuting Yang et al. (2019) recently provided a way to correct the surface resistance based on climate simulation outputs. However, this approach was not based on observational evidence nor physical principles and failed to fully resolve the PE overestimation issue noted in more recent studies (Berg & McColl, 2021; Liu et al., 2022; Vicente-Serrano et al., 2020).

Maybe a more fundamental problem of the current PE models stems from a paradoxical assumption itself. Assuming a saturated surface for any given meteorological conditions is paradoxical in that the overlying atmospheric conditions are not independent of land surface wetness due to land-atmosphere feedback processes (Kim et al., 2021; McColl et al., 2019; Rigden & Salvucci, 2017; Salvucci & Gentine, 2013). Since the warmer and drier future climate over land is already regulated by soil moisture (Berg et al., 2016; Dirmeyer et al., 2021), considering this apparent trend in current PE models as an increased demand that is independent of the land surface can lead to a "double-counting" of soil drying (Berg & Sheffield, 2018). Therefore, the rapid increase in PE suggested for warming climate conditions may in fact be a methodological artifact caused by the structure of current PE models that, in effect, ignore land-atmosphere feedback processes (Berg & Sheffield, 2018). Nevertheless, it is not clear to what extent land-atmosphere feedback can explain the PE overestimation issue, and crucially these ideas have not yet been investigated comprehensively using observational evidence.

Here, we directly assess how current PE models diverge from observed evaporative demand. Furthermore, we suggest a physically-based alternative PE model that constrains the upper limit of evaporation based on land-atmosphere coupling processes. In the following section, we derive the alternative model and discuss the theory behind it. We then compare our novel PE model with the most commonly used PE models including Penman-Monteith (Allen et al., 1998; Monteith, 1965), Priestley-Taylor (Priestley & Taylor, 1972), and an empirical model that calculates PE as proportional to available energy (hereafter the Milly-Dunne PE model (P. C. D. Milly & Dunne, 2016)).

Since applications of PE are broad and of great societal importance, we hierarchically evaluate the three current PE models along with our alternative PE model over a range of scales, and present these results at the field, watershed, and global scales. We first use in-situ field-scale observations from 212 eddy covariance tower sites worldwide contained in the FLUXNET2015 dataset representing over 1500 site-years (Pastorello et al., 2020) to test the performance of PE models in reproducing non-water-stressed evaporation and its sensitivity to temperature and relative humidity. This is followed by watershed scale assessment of model performance compared to water balance observations for 338 US watersheds (Duan et al., 2006) for the 1983-2020 period. We then examine global-scale changes in PE models from a historical reference period to the future period using 25 general circulation models (GCMs) that were included in Coupled Model Intercomparison Project Phase 5 (CMIP5) (Taylor et al., 2012). Through these analyses, we evaluate the causes underlying the differing responses of PE models to changing climatic conditions.

2 PE models

2.1 Alternative PE model based on land-atmosphere coupling theory

Terrestrial evaporation is constrained by soil moisture (supply-side) as well as climatic conditions (demand-side). Increasing soil moisture (i.e., supply) increases evaporation until evaporation approaches its maximum rate. At the maximum level of evaporation, additional soil moisture cannot increase evaporation further, and thus evaporation and soil moisture become independent of each other. This transition point is known as critical soil moisture (Denissen et al., 2020). Mathematically, this condition may be expressed as the derivative of evaporation (E) with respect to soil moisture (θ) $\frac{\partial E}{\partial \theta} = 0$.

The soil moisture control on terrestrial evaporation also interacts with the overlying atmosphere since the vertical gradient of relative humidity from the land surface to the atmosphere simultaneously changes with evaporation (Kim et al., 2021; Salvucci & Gentine, 2013). Soil moisture supply to a dry soil (i.e., soil wetting) increases relative humidity at the land surface (RH_0) at a faster rate than the change in atmospheric relative humidity (RH) (i.e., $\frac{\partial RH_0}{\partial \theta} > \frac{\partial RH}{\partial \theta}$), which leads to increased evaporation (**Figure 1**). As RH_0 approaches saturation, the increasing rate of RH_0 reduces, becoming limited by and converging into $\frac{\partial RH_0}{\partial \theta} = \frac{\partial RH}{\partial \theta}$, and thus evaporation reaches its maximum. Therefore, the maximum evaporation should satisfy not only $\frac{\partial E}{\partial \theta} = 0$ but also $\frac{\partial RH_0}{\partial \theta} = \frac{\partial RH}{\partial \theta}$ if considering the overlying air as a coupled system with the land surface.

In Appendix A, we provide a detailed derivation of $\frac{\partial E}{\partial \theta}$. Substituting $\frac{\partial E}{\partial \theta} = 0$ and $\frac{\partial RH_0}{\partial \theta} = \frac{\partial RH}{\partial \theta}$ into the derivative $\frac{\partial E}{\partial \theta}$ and then assuming $\frac{\partial RH_0}{\partial \theta} > 0$ yields

$$PE = \frac{2RHs+\gamma}{2RHs+2\gamma}\frac{R_n-G}{\lambda} \tag{1}$$

where, $s(=\frac{\partial q^*}{\partial T})$ is the linearized slope of saturation specific humidity versus temperature, γ is psychrometric constant, λ is the latent heat of vaporization, R_n is net radiation, G is soil heat flux, and R_n - G is available energy (AE) at the land surface.

Equation (1) represents a formulation for the upper limit of evaporation, and as such it can be considered an alternative PE model. Our proposed alternative has several unique characteristics. First, in deriving equation (1), the overlying air is considered as a coupled system with the land. Since relative humidity in the atmosphere is connected with the land surface dryness in our model, a decrease in relative humidity reduces evaporation in equation (1), which stands in contrast to the Penman-Monteith model. Second, the derivation of equation (1) does not assume a saturated land surface, and its physical meaning can be stated as the "evaporation rate that would take place under conditions where evaporation becomes independent of soil moisture". Third, while the current PE models require empirical parameters, equation (1) does not, and as such it does not require any parameter calibration. Fourth, the only required variables for calculating equation (1) are standard measurements (air temperature, relative humidity, and available energy).

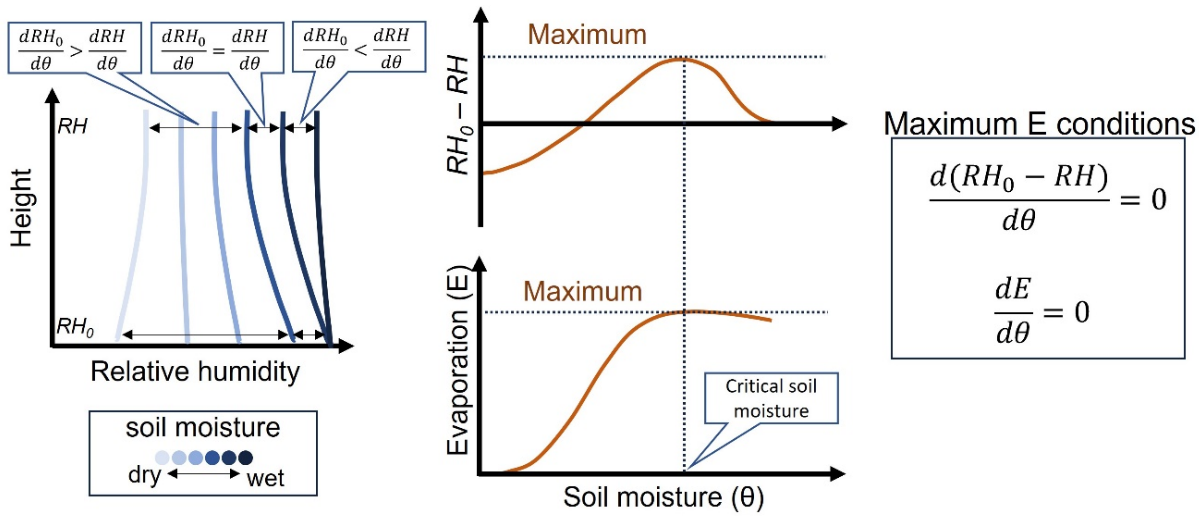

Figure 1. Conceptual framework of two mathematical constraints of the alternative PE model in Equation 1. The vertical profile of relative humidity evolves with soil moisture (θ). When soil is dry, the sensitivity of surface relative humidity (RH_0) to θ change is larger than the sensitivity of atmospheric relative humidity (RH) to changes in θ. Once θ approaches critical soil moisture, the two sensitivities become equivalent, and evaporation reaches its maximum.

2.2 Other PE formulations

We calculated Penman-Monteith PE based on the FAO reference crop method (Allen et al., 1998).

$$PE = \frac{s(R_n - G) + \rho c_p (q^*(T_a) - q_a)/r_a}{\lambda[s + \gamma(1 + r_s/r_a)]} \qquad (2)$$

where, $s(= \frac{\partial q^*}{\partial T})$ is the linearized slope of saturation specific humidity versus temperature, γ is psychrometric constant, λ is the latent heat of vaporization, R_n is net radiation, G is soil heat flux, ρ is air density, c_p is the specific heat capacity of the air, q^* is saturation specific humidity, q_a is air specific humidity, T_a is air temperature. r_s is surface resistance and set to 70 s m^{-1} based on the FAO method (Allen et al., 1998). r_a is aerodynamic resistance and calculated as $\frac{208}{u_2}$, where u_2 is 2 m height wind speed. u_2 was calculated based on FAO method (Allen et al., 1998) from wind speed and measurement height (z) as $u_2 = u_z \frac{4.87}{ln(67.8z - 5.42)}$.

We then calculated Priestley-Taylor PE as follows

$$PE = \alpha_{PT} \frac{s}{s + \gamma} \frac{R_n - G}{\lambda} \qquad (3)$$

where, α_{PT} is Priestley-Taylor coefficient and set to 1.26 (Priestley & Taylor, 1972).

Finally, we calculated Milly-Dunne PE as follows

$$PE = \alpha_{MD} \frac{R_n - G}{\lambda} \qquad (4)$$

where, α_{MD} is Milly-Dunne coefficient and set to 0.8 (P. C. D. Milly & Dunne, 2016).

3 Materials and Methods

We hierarchically evaluate our alternative PE model and the three current PE models (i.e., equations 1, 2, 3, and 4) over a range of scales, and present these results at the field, watershed, and global scales. All resulting figures were generated by using the R statistical language (R CORE TEAM, 2018). In the following subsections, we describe details of the dataset we used.

3.1 FLUXNET2015 in situ observations

The FLUXNET2015 dataset, which includes 212 empirical eddy-covariance flux tower sites around globe representing over 1,500 site years (Pastorello et al., 2020), was used for the site-scale analyses. Latent and sensible heat fluxes, net radiation, soil heat flux, air temperature, relative humidity, wind speed, and barometric pressure were obtained at weekly scales from the FLUXNET2015 dataset. We selected data only when all required variables for PE calculations are available. Bowen ratio corrected turbulent heat fluxes were used for this analysis following methods employed in previous analysis (Maes et al., 2019). Measurement heights for each site were also retrieved to calculate aerodynamic resistance for the Penman-Monteith model.

We only included data for periods for which the quality control flag indicated more than 80% of the half-hourly data were used for generating the daily or weekly datasets (i.e., measured data or good quality gap-filled data). Also, we filtered out data points when available energy (i.e., net radiation minus soil heat flux) was negative or local advection was strong (i.e., negative sensible heat flux) (Maes et al., 2019). Also, data in which surface energy imbalance (available energy minus sum of sensible and latent heat flux) was greater than 50 W m^{-2} were excluded.

Following a recent study (Maes et al., 2019; Tu et al., 2022), we isolated non-water-stressed conditions by selecting data with evaporative fraction (EF) exceeding 95% of each site's EF distribution. This selection strategy was adopted since soil moisture observations are only available for a few FLUXNET2015 sites, and previous research found no significant difference between soil moisture-based and EF-based criteria (Maes et al., 2019). The isolated non-water-stressed evaporation observations were used as a reference to assess the PE models. PE models were calculated based on equations (1, 2, 3, and 4) using observed meteorological variables at the flux towers. The bigleaf R package was used for anlaysing this flux dataset (Knauer et al., 2018).

3.2 US watersheds

For the watershed-scale analysis, watersheds included in MOPEX (Model Parameter Estimation Experiment) were analyzed (Duan et al., 2006). We selected MOPEX watersheds for which more than 30 years of runoff observations are available for the period of 1983-2020. The total number of watersheds meeting the criterion was 338, resulting in over 10,000 watershed-years of runoff observations. We first calculated uncorrected annual evaporation as the difference between observed precipitation based on the PRISM dataset (Daly et al., 1994) and USGS runoff observations on a water-year (i.e., October 1 to September 30) basis. Groundwater storage changes for each watershed were then estimated by the average storage changes of the two reanalysis datasets which provide all water balance components (i.e., ERA5-Land (Hersbach et al., 2020) and FLDAS (McNally et al., 2017) datasets). We then corrected annual scale watershed evaporation based on the mean estimated storage change from ERA5-Land and FLDAS.

Maximum annual evaporation for the 1983-2020 period for each watershed was used as a reference to assess the PE models. At the watershed scale, PE models are calculated based on equations (1, 2, 3, and 4) using monthly meteorological variables retrieved from ERA5-Land (Hersbach et al., 2020) and FLDAS (McNally et al., 2017) datasets. Here, we assumed that soil heat flux is zero. PE values were calculated by the average of the two reanalysis datasets. In order to analyze relationship between PE and soil moisture, we obtained soil moisture derived by the SMAP (Soil Moisture Active Passive) satellite mission and calculated annual mean percent soil moisture for each watershed using the NASA-USDA Enhanced SMAP dataset (Mladenova et al., 2020). The soil moisture, precipitation, and reanalysis datasets were downloaded from Google Earth Engine (Gorelick et al., 2017) using the rgee R package (Aybar et al., 2020), while the USGS runoff observations were downloaded using the dataRetrieval R package (De Cicco et al., 2018).

3.3 CMIP5 simulations

For the global-scale analysis, we used 25 publicly available GCMs that participated in CMIP5. Although Coupled Model Intercomparison Project Phase 6 (CMIP6) models recently became publicly available, we used CMIP5 models to enable comparison of this study with the relevant previous studies (Berg & McColl, 2021; P. C. D. Milly & Dunne, 2016; Yuting Yang et al., 2019). Latent and sensible heat fluxes, air temperature, relative humidity, wind speed, barometric pressure, precipitation, runoff, and evaporation were obtained from the models' outputs. CMIP5 models that provide all required variables for the PE calculations were selected, and the models include: ACCESS1-0, ACCESS1-3, CNRM-CM5, GISS-E2-R-CC, HadGEM2-CC, HadGEM2-ES, bcc-csm1-1, bcc-csm1-1-m, CanESM2, CESM1-CAM5, CSIRO-Mk3-6-0, GFDL-CM3, GFDL-ESM2G, GFDL-ESM2M, GISS-E2-H, GISS-E2-H-CC, GISS-E2-R, inmcm4, IPSL-CM5A-LR, IPSL-CM5A-MR, IPSL-CM5B-LR, MIROC-ESM, MIROC-ESM-CHEM, MIROC5, and MRI-CGCM3. These CMIP5 models' output were obtained from the Columbia University Lamont-Doherty Ocean and Climate Physics Data Library (http://strega.ldeo.columbia.edu:81/CMIP5/).

We used monthly outputs of the historical reference period (1981-2000) and the high emission future period (2081-2100 under RCP 8.5) to calculate the mean values of each period for PE, precipitation, and runoff. In order to calculate the multimodel mean and median, the models were regridded to a 2°×2° resolution (Berg & McColl, 2021). Runoff output is not available for some models (the first six models in the above model list); in these cases, we estimated runoff as the difference between precipitation and evaporation (P. C. D. Milly & Dunne, 2016).

PE models were calculated based on equations (1, 2, 3, and 4) using monthly CMIP5 models' meteorological output, and then aggregated into 20 years average for the historical and future periods, respectively. Since soil heat flux is not available in CMIP5 model outputs, we calculated available energy (i.e., net radiation minus soil heat flux) as the sum of latent and sensible heat fluxes following recent studies (Berg & McColl, 2021; P. C. D. Milly & Dunne, 2016). We calculated PE only for the land fraction which does not include Greenland and Antarctica (Berg & McColl, 2021; P. C. D. Milly & Dunne, 2016).

3.4 Budyko model

To evaluate hydrological implications of the varying increasing rates of the different PE models estimated by CMIP5 models, we estimated runoff (Q) based on the Budyko water balance model, which is forced by PE and precipitation (P). The Budyko water balance model can be written following (P. C. D. Milly & Dunne, 2016)

$$Q = P - P[\frac{PE}{P} tanh \frac{P}{PE}(1 - cosh \frac{PE}{P} + sinh \frac{PE}{P})]^{\frac{1}{2}} \quad (5)$$

In this equation, all variables should be understood as 20 year mean values over the historical or future periods. Although there are several functions representing the Budyko model, we select this original equation following P. C. D. Milly and Dunne (2016). We also tested an equation used by Yuting Yang et al. (2019), and found similar results, implying choice of the Budyko equation may be a minor issue at global scale although prediction skill can be improved at a regional scale.

4 Results and Discussion

4.1 Site-level evaluation 1: performance

The performances of PE models are evaluated using FLUXNET2015 in-situ observations around globe (Pastorello et al., 2020). We isolated weekly scale evaporation observations for non-water-stressed conditions by selecting periods with high evaporation relative to available energy, an approach based on a recent study (Maes et al., 2019) (Methods). The observed values of non-water-stressed evaporation (E_{unstr}) are used as a reference of the upper limit to evaporation to assess the PE models (Penman-Monteith (PM), Priestley-Taylor (PT), Milly-Dunne (MD), and equation (1)) since PE should become equivalent to actual evaporation under non-water-stressed conditions. We found that equation (1) most accurately reproduces observed E_{unstr} in terms of root mean square error (RMSE), coefficient of determination (R^2), and regression slope relative to current PE models (**Figure 2 a-d**). The MD PE model yielded similar site-scale performance with equation (1), while the widely used PM PE showed the lowest performance.

Importantly, equation (1) does not show significant bias regarding temperature and relative humidity, unlike biases present in all current PE models (**Figure 2 e-h**). For example, the PM and PT models overestimate observed E_{unstr} when the temperature is high and/or relative humidity is low. Our findings for the PM and PT models are consistent with the PE overestimation bias first reported by Milly and Dunne (P.C.D. Milly & Dunne, 2017) for models used to predict PE under future climate conditions. In contrast, our PE model exhibits the smallest bias with respect to temperature and relative humidity, making it more appropriate for PE calculations when evaluating future climate scenarios in frameworks that use PE as a parameter.

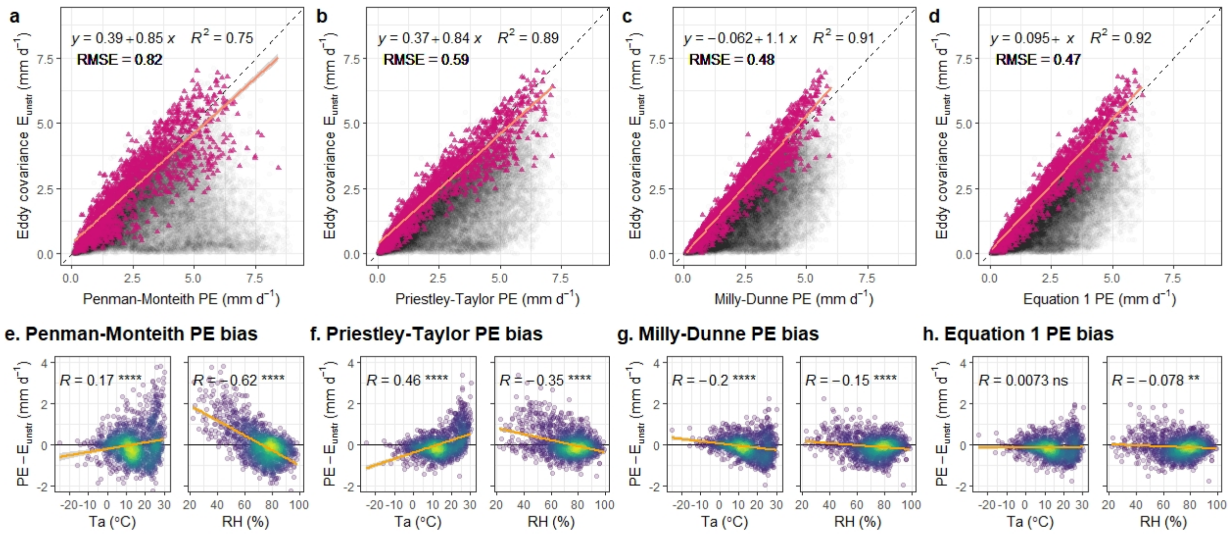

Figure 2. Observed non-water-stressed evaporation predicted by PE models, and their bias. From **a** to **d**, the y-axis is weekly observations of non-water-stressed evaporation (E_{unstr}), and the x-axis is PE calculated by Penman-Monteith, Priestley-Taylor, Milly-Dunne, and equation (1), respectively. Shaded points represent all evaporation observations while coloured triangles represent E_{unstr}. The regression lines are based only on the coloured triangles. From **e** to **h**, biases of each model (y-axis) are depicted as a function of air temperature (T_a) and relative humidity (RH).

4.2 Site-level evaluation 2: climate sensitivity of PE

We then use multiple-linear regression to determine the sensitivity of PE models to temperature ($\frac{\partial PE}{\partial T}$) and to relative humidity ($\frac{\partial PE}{\partial RH}$). Regression slopes for each PE model and E_{unstr} are considered as the sensitivity in **Figure 3 a-b**. It should be noted that since we only use temperature and relative humidity as independent variables, these sensitivities represent not only direct effects (e.g., saturation vapour pressure) but also indirect effects (e.g., net radiation).

The PT model yielded the largest overestimates of observed E_{unstr} sensitivity to increasing temperature. Of the four PE models, the PM model was found to be the most largely biased for RH ($\frac{\partial PE}{\partial RH}$) compared to the observed sensitivity of E_{unstr} to RH. These results show how the PM and PT models overestimate evaporative demand in warmer and drier future climates. On the other hand, equation (1) exhibits good performance in reproducing observed sensitivity to temperature and relative humidity.

To further understand the influence of temperature and relative humidity on each PE model, we depict each PE model's evaporative fraction (EF) in **Figure 3 c-e**, where EF represents the ratio of evaporation to available energy. Here, EF for Milly-Dunne's model is fixed at a constant 0.8 by definition (dashed line). Increases in temperature result in increasing EF for the remaining three PE models (equation (1), PM and PT) due to the saturation vapour pressure effect, but EF computed with our proposed model increases only modestly compared to the PM and PT models. Also, the EF determined with equation (1) decreases as relative humidity declines, since relative humidity reflects land surface dryness. As a result, EF determined with equation (1) covers a much narrower range of values than the PM and PT models, with values centered on Milly-Dunne's 0.8 fixed value of EF. In contrast, the Penman-Monteith model's EF rapidly increases for declining relative humidity due to the surface saturation assumption, and it is probably the key reason for the relatively poor performance of the PM model.

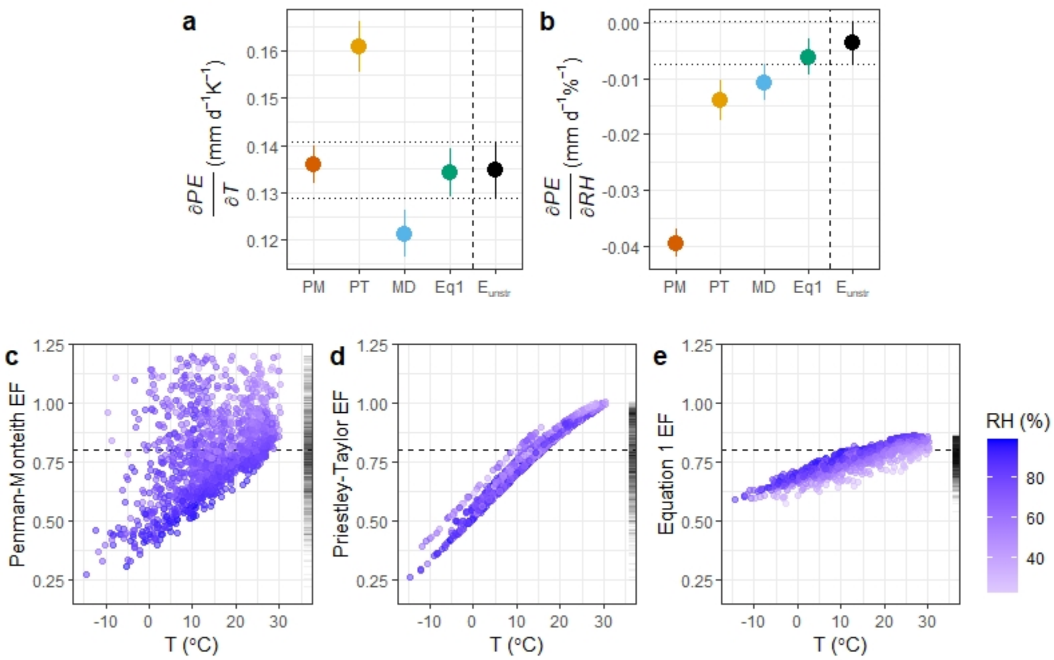

Figure 3. Climate sensitivities of PE models and measured evaporation for non-water-stressed periods (E_{unstr}) (a-b) and evaporative fraction (EF) of PE models as a function of climate variables (c-e). From **a** to **b**, the y-axis of each panel is the PE sensitivities to temperature (T) and to relative humidity (RH), respectively. The error bar indicates 2 standard error, and the dotted lines represent the E_{unstr} error bar range. From **c** to **e**, the y-axis of each panel is EF of Penman-Monteith, Priestley-Taylor, and equation (1), respectively. The dashed line in panels c-e represents Milly-Dunne EF (fixed at 0.8). The short black lines on the right-side margins of panels c-e shows EF distributions for PM EF, PT EF, and Equation 1 EF, respectively.

4.3 Watershed-level evaluation 1: performance

We then evaluated the performance of the four PE models (PM, PT, MD and equation (1)) using runoff observations from 338 US watersheds for the period of 1983-2020 (Duan et al., 2006). Annual evaporation was estimated as the difference between observed precipitation (PRISM dataset (Daly et al., 1994)) and USGS runoff observations considering groundwater storage change (Materials and Methods). Maximum annual evaporation for the 1983-2020 period for each watershed was selected and used as a validation criterion for the PE models which were parameterized using two reanalysis datasets: ERA5-Land (Hersbach et al., 2020) and FLDAS (McNally et al., 2017). As depicted in **Figure 4**, equation (1) most accurately reproduces observed maximum watershed evaporation, as an indicator of upper limit of evaporation, in terms of RMSE, R^2, and regression slope, while the PM model leads to the least accurate results. These watershed-scale results are consistent with the results we obtained for the site-level analysis.

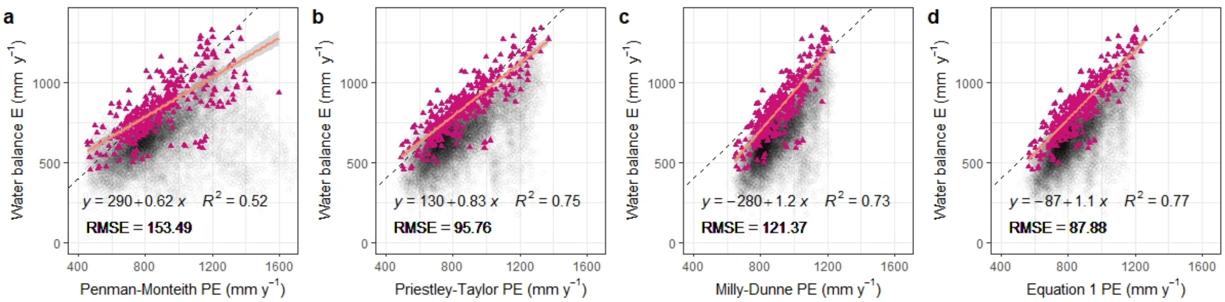

Figure 4. Observed maximum annual evaporation at US watersheds predicted by PE models. From **a** to **d**, the y-axis is annual water balance evaporation for each of 338 watersheds, and the x-axis is PE calculated by Penman-Monteith, Priestley-Taylor, Milly-Dunne, and our proposed model, respectively. Shaded points represent annual water balance evaporation while coloured triangles represent maximum annual evaporation for each watershed. The regression lines are based only on the coloured triangles.

4.4 Watershed-level evaluation 2: evaporation sensitivity to PE

Using the long-term watershed observations, we evaluate the sensitivity of annual scale evaporation to each PE model ($\frac{\partial E}{\partial PE}$). We use multiple-linear regression to determine the sensitivity of evaporation to PE and to precipitation (P) assuming evaporation is constrained by precipitation (supply-side) as well as PE (demand-side). Regression slopes are considered as the sensitivity. Theoretically, dry watershed ($\frac{P}{PE} < 1$) evaporation is largely determined by precipitation while wet watershed ($\frac{P}{PE} > 1$) evaporation is primarily determined by PE. Therefore, $\frac{\partial E}{\partial PE}$ should be around zero to one for dry watersheds while $\frac{\partial E}{\partial PE}$ should be close to one for wet watersheds.

For wet watersheds, where the role of PE is important in controlling evaporation, $\frac{\partial E}{\partial PE}$ determined by MD model and equation (1) are aligned with this theoretical expectation while the PM model is not (**Figure 5a**). PM model's $\frac{\partial E}{\partial PE}$ is significantly less than unity for most wet watersheds, meaning changes in PE are always larger than changes in evaporation. This finding implies that future evaporation can be overestimated if evaporation is constrained by the PM PE model even for wet watersheds.

Is there any theoretical reason underlying this result? Fundamentally, terrestrial evaporation is constrained by soil moisture limitations (supply) and PE (demand), and thus one can write evaporation as $E = f_{sm}PE$, where f_{sm} represents the soil moisture constraint ranging from zero to one. Therefore, the sensitivity of evaporation to PE can be written as follows.

$$\frac{\partial E}{\partial PE} = \frac{\partial f_{sm}}{\partial PE}PE + f_{sm} \quad (6)$$

If f_{sm} and PE are independent, the first term becomes negligible, and thus one can write $\frac{\partial E}{\partial PE} = f_{sm}$. For wet watersheds, f_{sm} is close to one and thus $\frac{\partial E}{\partial PE}$ becomes one in principle. On the other hand, if f_{sm} and PE have a negative correlation, $\frac{\partial E}{\partial PE}$ cannot approach one even for wet watersheds due to the first term in equation (6). As depicted in **Figure 5 b-e**, the PM model shows the most apparent negative relationship with satellite-derived soil moisture (Mladenova et al., 2020), which explains why $\frac{\partial E}{\partial PE}$ does not generally approach one using the PM model, even for wet watersheds. In contrast, MD model and equation (1) do not show an apparent dependency on soil moisture.

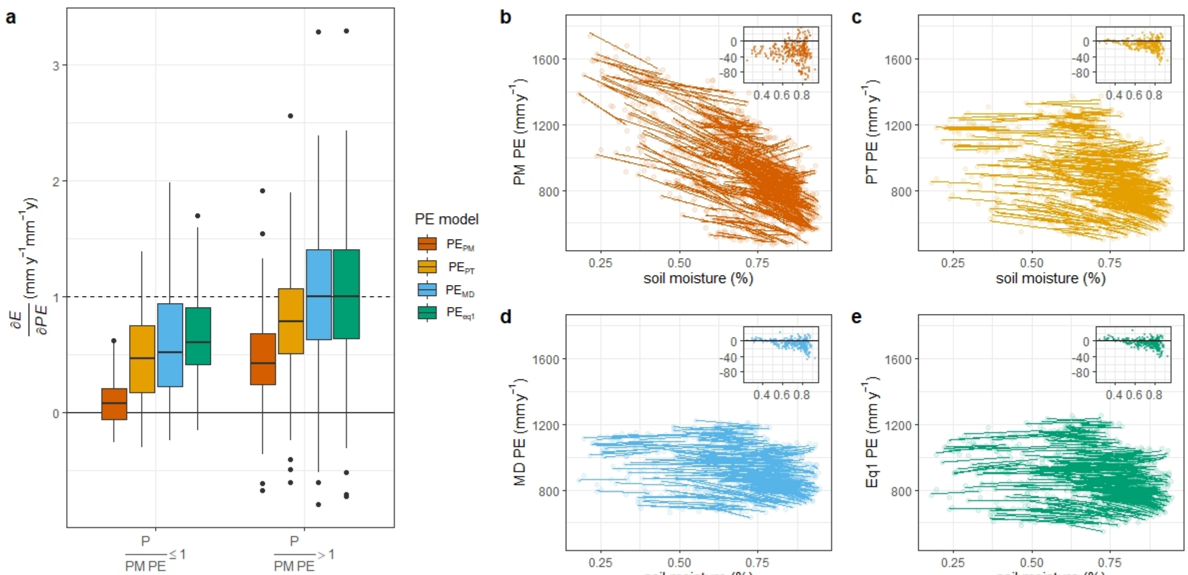

Figure 5. Sensitivities of watershed annual evaporation to PE models (a) and relationship between PE models and soil moisture (b-e). a. each watershed sensitivity is group by ratio between precipitation and the PM PE. From **b** to **e**, the y-axis is Penman-Monteith, Priestley-Taylor, Milly-Dunne, and our proposed model, respectively, and the x-axis is annual mean percent soil moisture retrieved by the NASA-USDA enhanced SMAP product. Each regression line represents one of the 338 watershed. The inset shows the slope of each regression line.

4.5 Projections of the PE models to anthropogenic climate change

Following P. C. D. Milly and Dunne (2016), we compared century-scale changes in PE models from a historical reference period (1981-2000) to a future scenario (2081-2100) using 25 CMIP5 models under Representative Concentration Pathway 8.5 (Methods and Table S1). The four tested PE models suggest increasing PE over most of the terrestrial regions for the future relative to the reference period, but the magnitude of the changes vary substantially. Consequently, projected median PE changes over the global land surface vary, from smallest to largest: Milly-Dunne (52 mm yr^{-1}), equation (1) (75 mm yr^{-1}), Priestley-Taylor (125 mm yr^{-1}), and Penman-Monteith (224 mm yr^{-1}) (**Figure 6**). These differences originate from the EF responses to future climatic conditions represented by the individual PE models. Both rising temperatures and declining relative humidity result in increased Penman-Monteith EF, and hence the largest increase in PE is projected by the PM PE model. For the Priestley-Taylor model, EF is not directly affected by relative humidity, while rising temperatures increase EF. Thus, the projected mean increase in PT PE is lower than for the PM PE model. In contrast, declining relative humidity projected for future climate conditions results in reduced EF with equation (1), and thus PE changes projected in the present study are lower than those obtained using PT and PM models.

We considered changes in ocean evaporation projected by GCMs as a reference point for changes in non-water-limited evaporation under future climatic conditions. The median change in ocean evaporation is about 76 mm yr^{-1}, which is most closely matched by our PE model (**Figure 6**). Over the ocean, temperatures are increasing at a slower rate than for the land. Also, relative humidity is roughly steady over the ocean, unlike the declining trend in RH over land, a difference known as the "land-ocean contrast" (Byrne & O'Gorman, 2016, 2018). "Land-ocean contrast" effects on evaporative demand can be reconciled using equation (1) because the influence of temperature on EF is conditioned by changes in relative humidity. This is a reason why our proposed PE model is well-matched with the ocean evaporation change. However, in the PM PE model, the "land-ocean contrast" increases PE unrealistically compared to the ocean evaporation, resulting in a projected change in PE for the land surface that is nearly 3X that projected for evaporation from the ocean.

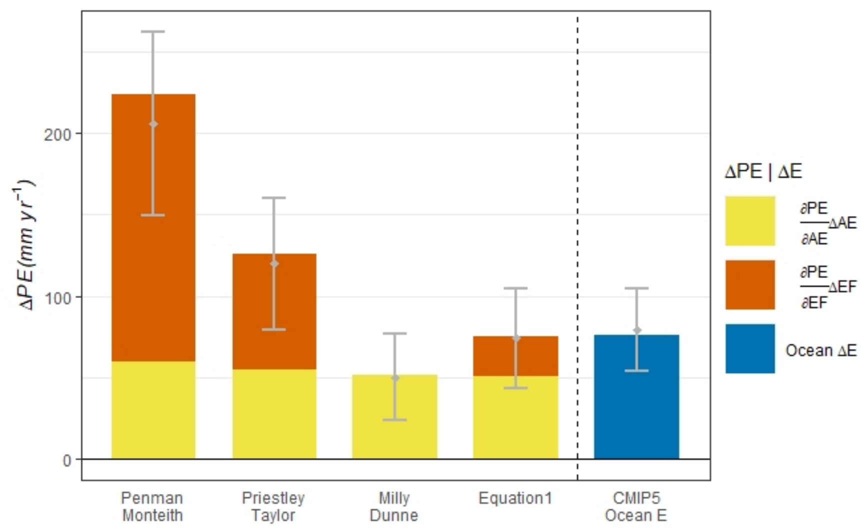

Figure 6. Global scale changes in PE in the future period 2081-2100 (RCP 8.5) relative to the historic period 1981-2000. The bars represent the ensemble median of 25 CMIP5 models while the points and error bars indicate the ensemble mean ±1 standard deviation. Changes in different PE models and their components are presented and change in ocean evaporation is presented for reference. Here, EF is evaporative fraction and AE is available energy.

4.6 Varying runoff projections resulting from the different PE models

In order to evaluate hydrological implications of the varying increasing rates of the different PE models, we compared runoff changes estimated using the Budyko water balance approach forced by PE and precipitation (**Figure 7**), following P. C. D. Milly and Dunne (2016) (Methods). The Budyko-estimated runoff change forced with our proposed PE model (15 mm yr^{-1} at global scale) most closely matches the direct CMIP5 projections (17 mm yr^{-1}). The Milly-Dunne PE based Budyko runoff change (23 mm yr^{-1}) slightly overestimates the direct CMIP5 projections. In contrast, when the Penman-Monteith model is used, the Budyko estimated runoff change (-2 mm yr^{-1}) largely underestimates the direct CMIP5 output. The Priestley-Taylor model

(5 mm yr^{-1}) is a better comparator with CMIP5 than Penman-Monteith, but it still underestimates the direct CMIP5 projections.

In terms of spatial patterns, the Budyko-estimated runoff forced with the PM PE model shows apparent bias while other models show reasonable agreement with the direct CMIP5 projections. Especially, the PM PE model shows a large negative bias in wet regions such as the tropics. As we demonstrated in the watershed scale analysis (**Fig. 5** and section 4.4), the PM PE model overestimates evaporation increase particularly for wet watersheds, where the role of PE is important in controlling evaporation. Therefore, evaporation increases could be largely overestimated in wet regions if one applies the PM PE model, which results in a large negative bias in runoff projections for the wet regions. This runoff projections bias can be reduced using the PT PE model and further reduced using the MD PE model and equation (1).

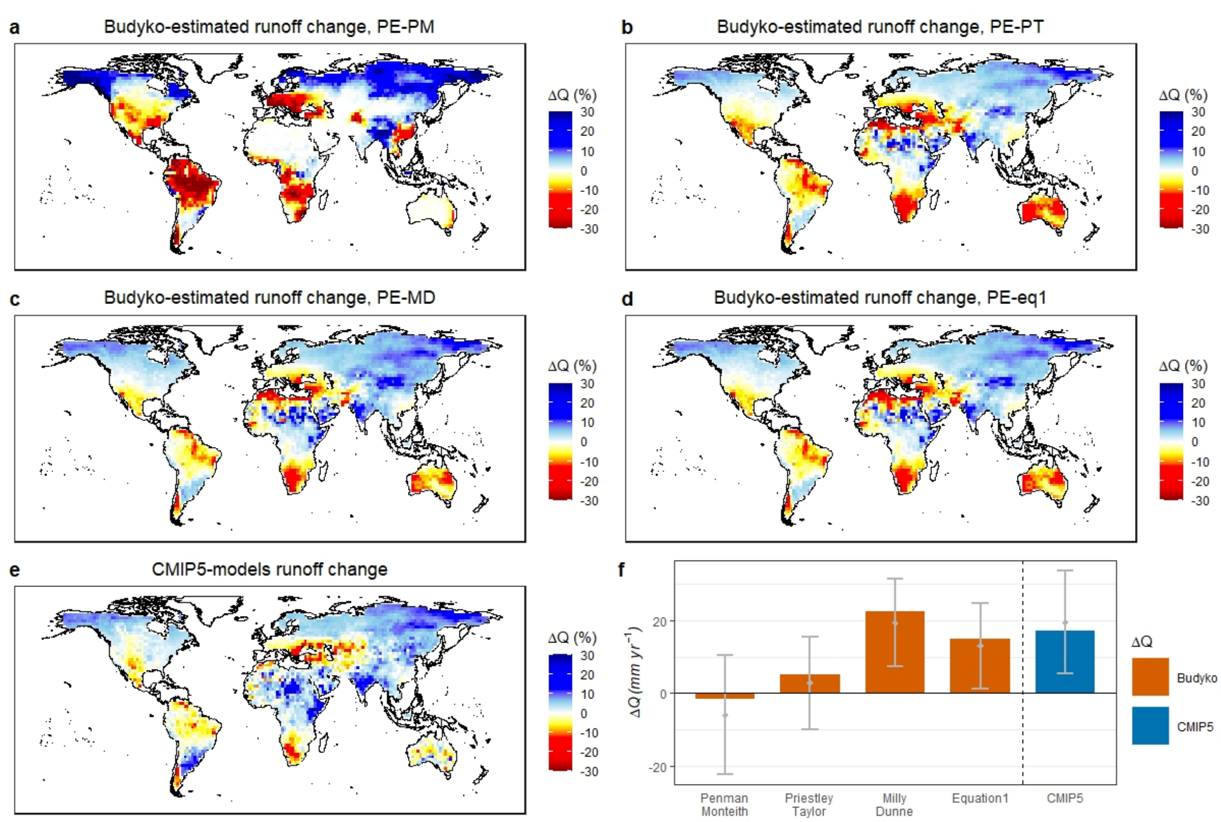

Figure 7. Multi CMIP5 models median of the relative change of the annual mean runoff (a-e), and global scale changes runoff (f) in the future period 2081-2100 (RCP 8.5) relative to the historic period 1981-2000. From **a** to **d**, runoff change estimated by Budyko model forced by each PE model while **e.** represents direct CMIP5 models' output. Here, relative change indicates future minus historical divided by average of historical and future. **f.** Changes in runoff estimated by the Budyko model using different PE models and change in runoff directly projected by CMIP5 is presented for reference. The bars represent the ensemble median of 25 CMIP5 models while the points and error bars indicate the ensemble mean ±1 standard deviation.

5 Discussion and conclusions

Although warmer and drier air is widely recognized to correspond to high atmospheric evaporative demand, the terrestrial supply-side mechanism constraining atmospheric aridity tends to be overlooked. That is, soil moisture represents a supply constraint to warmer and drier air through the land-atmosphere feedback. This feature is ignored in current PE models which assumes a saturated surface for any given meteorological condition. As such, current PE models untenably overestimate evaporative demand for warmer and drier conditions and thus overestimate evaporation change, even for non-water limited conditions. The systematic biases of current PE models have serious implications that could lead to inappropriate planning in relation to needed climate change mitigation and adaptation. Arguably, to fundamentally resolve this problem, one should consider the overlying atmosphere as a coupled system with the land surface instead of solely as a source of evaporative demand that is independent from terrestrial processes.

Perhaps, current PE models would be still essential tools for some purposes (Vicente-Serrano et al., 2020). For instance, the PM PE model could be a useful indicator of wildfire risk in that high PM PE values represent drier air (Y. Huang et al., 2020; McEvoy et al., 2020). It should be noted that our analyses are not intended to deny or replace the various applications of these PE models. However, if the current PE model is used as evaporative demand that controls actual evaporation and evapotranspiration or other water balance components, the systematic biases toward drying are unavoidable under anthropogenic climate change. Therefore, care should be taken while applying and interpreting the PE models.

Internally consistent climate simulations that incorporate coupled land-ocean-atmosphere processes such as GCMs can be a solution to this issue. However, these sophisticated simulations and low-resolution outputs cannot fully replace widely used operational approaches based on PE such as watershed hydrological models, crop growth and crop water use models, drought and aridity analysis, and global satellite-based evaporation products (e.g. MOD16, GLEAM or PT-JPL). By presenting a land-atmosphere coupled PE model that can be easily implemented in established hydrologic approaches using readily measurable parameters, we believe that the land-atmosphere coupling perspective can be effectively implemented into a wide range of hydrological planning tools, particularly those focused on evaluating responses to changing climatic conditions.

Appendix A: the derivative of evaporation with respect to soil moisture

Vertical water vapour flux from the earth's surface (i.e., evaporation) is constrained by the difference in specific humidity (q) between the land surface and the atmosphere. If we express specific humidity as the product of saturation specific humidity and relative humidity, evaporation can be written as follows.

$$\lambda E = \lambda\rho \frac{RH_0 q^*(T_0) - RH_a q^*(T_a)}{r_a} \quad \text{(A1)}$$

where, E is evaporation, λ is the latent heat of vaporization, ρ is air density, q^* is saturation specific humidity, T is temperature, RH is relative humidity, r_a is aerodynamic resistance to water vapour transfer (s m^{-1}). The subscript a indicates the atmospheric state near the land surface, and the subscript 0 indicates the land surface. The derivative of E with respect to soil moisture (θ) can be expressed as follows.

$$\lambda \frac{\partial E}{\partial \theta} = \frac{\lambda\rho}{r_a}\left(RH_0 s \frac{\partial T_0}{\partial \theta} - RH_a s \frac{\partial T_a}{\partial \theta} + q^*(T_0)\frac{\partial RH_0}{\partial \theta} - q^*(T_a)\frac{\partial RH_a}{\partial \theta}\right) \quad \text{(A2)}$$

where, $s(=\frac{\partial q^*}{\partial T})$ is the linearized slope of saturation specific humidity versus temperature (kg water vapour (kg moist air)$^{-1}$ K^{-1}). We assume identical s for the land surface and the atmosphere as is typically assumed in evaporation models. Also, we assume that r_a is independent to soil moisture.

The land surface state and the atmospheric state can be related as follows.

$$dT_a = dT_0 - d(T_0 - T_a) \quad \text{(A3)}$$

$$dRH_a = dRH_0 - d(RH_0 - RH_a) \quad \text{(A4)}$$

Substituting equations (A3) and (A4) into equation (A2) yields

$$\lambda \frac{\partial E}{\partial \theta} = \left(\lambda\rho s \frac{RH_0 - RH_a}{r_a}\right)\frac{\partial T_0}{\partial \theta} + \frac{\lambda\rho RH_a s}{r_a}\frac{\partial (T_0 - T_a)}{\partial \theta} + \left(\lambda\rho \frac{q^*(T_0) - q^*(T_a)}{r_a}\right)\frac{\partial RH_0}{\partial \theta} + \frac{\lambda\rho q^*(T_a)}{r_a}\frac{\partial (RH_0 - RH_a)}{\partial \theta} \quad \text{(A5)}$$

If we approximate $q^*(T_0) - q^*(T_a) \approx s(T_0 - T_a)$ and assume identical r_a for water vapour and sensible heat transfer, the second and the third terms of the right-hand side of equation (A5) can be expressed using sensible heat flux (i.e., $H = \rho c_p \frac{T_0 - T_a}{r_a}$).

$$\lambda \frac{\partial E}{\partial \theta} = \left(\lambda\rho s \frac{RH_0 - RH_a}{r_a}\right)\frac{\partial T_0}{\partial \theta} + \frac{RH_a s}{\gamma}\frac{\partial H}{\partial \theta} + \frac{s}{\gamma} H \frac{\partial RH_0}{\partial \theta} + \frac{\lambda\rho q^*(T_a)}{r_a}\frac{\partial (RH_0 - RH_a)}{\partial \theta} \quad \text{(A6)}$$

where, $\gamma(=\frac{c_p}{\lambda})$ is the psychrometric constant and c_p is the specific heat capacity of the air. We then substitute the energy balance equation (i.e., $H = (R_n - G) - \lambda E$) into the second and the third terms of the right-hand side of equation (A6), and then arrange it as follows.

$$\lambda \frac{\partial E}{\partial \theta} = \left(\rho c_p \frac{RH_0 - RH_a}{r_a}\right)\frac{s}{RH_a s + \gamma}\frac{\partial T_0}{\partial \theta} + \frac{RH_a s}{RH_a s + \gamma}\frac{\partial (R_n - G)}{\partial \theta} + [(R_n - G) - E]\frac{s}{RH_a s + \gamma}\frac{\partial RH_0}{\partial \theta} + \frac{\rho c_p q^*(T_a)}{(RH_a s + \gamma) r_a}\frac{\partial (RH_0 - RH_a)}{\partial \theta} \quad \text{(A7)}$$

Next, we replace T_0 with moist static enthalpy in conjunction with RH_0. Here, moist static enthalpy is known as $dh_0 = c_p dT_0 + \lambda dq_0$. If we express specific humidity as a multiplication of q^* and RH, moist static enthalpy can be written as $dh_0 = (c_p + \lambda RH_0 s)dT_0 + \lambda q^*(T_0)dRH_0$.

Thus, temperature change can be written as $dT_0 = \frac{1}{\lambda(RH_0 s+\gamma)} dh_0 - \frac{q^*(T_0)}{RH_0 s+\gamma} dRH_0$. Substituting this equation into the first term of the right-hand side of equation (A7) yields

$$\lambda \frac{\partial E}{\partial \theta} = [\frac{\rho s \gamma}{(RH_0 s+\gamma)(RH_a s+\gamma)} \frac{RH_0 - RH_a}{r_a}] \frac{\partial h_0}{\partial \theta} + \frac{RH_a s}{RH_a s+\gamma} \frac{\partial (R_n - G)}{\partial \theta} + [\frac{RH_0 s+\gamma}{RH_a s+\gamma}(R_n - G - \lambda E) - \frac{\rho c_p q^*(T_0)}{RH_a s+\gamma} \frac{RH_0 - RH_a}{r_a}] \frac{s}{RH_0 s+\gamma} \frac{\partial RH_0}{\partial \theta} + \frac{\rho c_p q^*(T_a)}{(RH_a s+\gamma) r_a} \frac{\partial (RH_0 - RH_a)}{\partial \theta} \quad \text{(A8)}$$

We now assume $\frac{\partial h_0}{\partial \theta} = 0$ and $\frac{\partial (R_n - G)}{\partial \theta} = 0$, since incoming energy to the land surface and consequential moist static enthalpy can be considered as independent to soil moisture. Therefore, the first and second terms of the right-hand side of equation (A8) can be considered as negligible. Also, if we approximate $\frac{RH_0 s+\gamma}{RH_a s+\gamma} \approx 1$ in the third term, equation (A8) becomes as follows:

$$\lambda \frac{\partial E}{\partial \theta} = [(R_n - G) - \lambda E - \frac{\rho c_p q^*(T_0)}{RH_a s+\gamma} \frac{RH_0 - RH_a}{r_a}] \frac{s}{RH_0 s+\gamma} \frac{\partial RH_0}{\partial \theta} + \frac{\rho c_p q^*(T_a)}{(RH_a s+\gamma) r_a} \frac{\partial (RH_0 - RH_a)}{\partial \theta} \quad \text{(A9)}$$

Next, we substitute the PM_{rh} actual evaporation model (Kim et al., 2021) to the first term of the right-hand side of equation (A9). Here, the PM_{rh} evaporation model provides an equation for relative humidity flux (i.e., $\frac{\rho c_p q^*(T_0)}{RH_a s+\gamma} \frac{RH_0 - RH_a}{r_a} = \lambda E - \frac{RH_a s (R_n - G)}{RH_a s+\gamma}$). Therefore, equation (A9) becomes

$$\lambda \frac{\partial E}{\partial \theta} = [\frac{2RH_a s+\gamma}{2RH_a s+2\gamma}(R_n - G) - \lambda E] \frac{2s}{RH_0 s+\gamma} \frac{\partial RH_0}{\partial \theta} + \frac{\rho c_p q^*(T_a)}{(RH_a s+\gamma) r_a} \frac{\partial (RH_0 - RH_a)}{\partial \theta} \quad \text{(A10)}$$

Equation (A10) can be solved for *E* by substituting $\frac{\partial E}{\partial \theta} = 0$ and $\frac{\partial RH_0}{\partial \theta} = \frac{\partial RH}{\partial \theta}$ and then assuming $\frac{\partial RH_0}{\partial \theta} > 0$, which yields

$$\lambda E = \frac{2RH_a s+\gamma}{2RH_a s+2\gamma}(R_n - G) \quad \text{(A11)}$$

Equation (A11) is exactly equivalent to equation (1) in the main text. It should be noted that we simplify RH_a to RH in the main text.

Acknowledgments

We express our thanks to the data providers, site investigators and technicians without who this effort would not have been possible. We want to thank Brenda D'Acunha, Stephen Chignell and Emily Mistick for helping with watershed data processing. We acknowledge the support of the Canadian Space Agency (CSA) Grant 21SUESIELH.

Conflict of Interest

The authors declare that they have no conflicts of interest.

Open Research

Data Availability Statement

All data described in the main text are available. The FLUXNET2015 dataset is available from FLUXNET (https://fluxnet.org/data/fluxnet2015-dataset/). The US watershed runoff dataset is available at https://waterservices.usgs.gov/. The PRISM precipitation, SMAP soil moisture and the two reanalysis datasets (ERA5-Land and FLDAS) are publicly available and can be accessed using tools such as Google Earth Engine (https://doi.org/10.1002/2015WR017031). All climate model simulations are from CMIP5 and are publicly available, and are hosted on various servers including the Columbia University Lamont-Doherty Ocean and Climate Physics Data Library (http://strega.ldeo.columbia.edu:81/CMIP5/).

References

Allen, R. G., Pereira, L. S., Raes, D., & Smith, M. (1998). Crop evapotranspiration-Guidelines for computing crop water requirements-FAO Irrigation and drainage paper 56. *FAO, Rome, 300*(9).

Ault, T. R. (2020). On the essentials of drought in a changing climate. *science, 368*(6488), 256-260. https://doi.org/10.1126/science.aaz5492

Aybar, C., Wu, Q., Bautista, L., Yali, R., & Barja, A. (2020). rgee: An R package for interacting with Google Earth Engine. *Journal of Open Source Software, 5*(51), 2272. https://doi.org/10.21105/joss.02272

Berdugo, M., Delgado-Baquerizo, M., Soliveres, S., Hernández-Clemente, R., Zhao, Y., Gaitán, J. J., et al. (2020). Global ecosystem thresholds driven by aridity. *science, 367*(6479), 787-790. https://doi.org/10.1126/science.aay5958

Berg, A., Findell, K., Lintner, B., Giannini, A., Seneviratne, S. I., van den Hurk, B., et al. (2016). Land–atmosphere feedbacks amplify aridity increase over land under global warming. *Nature Climate Change, 6*(9), 869-874. https://doi.org/10.1038/nclimate3029

Berg, A., & McColl, K. A. (2021). No projected global drylands expansion under greenhouse warming. *Nature Climate Change*. https://doi.org/10.1038/s41558-021-01007-8

Berg, A., & Sheffield, J. (2018). Climate change and drought: the soil moisture perspective. *Current Climate Change Reports, 4*(2), 180-191. https://doi.org/10.1007/s40641-018-0095-0

Byrne, M. P., & O'Gorman, P. A. (2016). Understanding decreases in land relative humidity with global warming: conceptual model and GCM simulations. *Journal of Climate, 29*(24), 9045-9061. https://doi.org/10.1175/jcli-d-16-0351.1

Byrne, M. P., & O'Gorman, P. A. (2018). Trends in continental temperature and humidity directly linked to ocean warming. *Proceedings of the National Academy of Sciences, 115*(19), 4863-4868. https://doi.org/10.1073/pnas.1722312115

Dai, A. (2013). Increasing drought under global warming in observations and models. *Nature Climate Change, 3*(1), 52-58. https://doi.org/10.1038/nclimate1633

Daly, C., Neilson, R. P., & Phillips, D. L. (1994). A statistical-topographic model for mapping climatological precipitation over mountainous terrain. *Journal of applied meteorology and climatology, 33*(2), 140-158. https://doi.org/10.1175/1520-0450(1994)033<0140:astmfm>2.0.co;2

De Cicco, L., Lorenz, D., Hirsch, R., & Watkins, W. (2018). dataRetrieval: R packages for discovering and retrieving water data available from US federal hydrologic web services. US Geological Survey, Reston, VA. https://doi.org/10.5066/P9X4L3GE

Denissen, J. M. C., Teuling, A. J., Reichstein, M., & Orth, R. (2020). Critical soil moisture derived from satellite observations over Europe. *Journal of Geophysical Research: Atmospheres, 125*(6), e2019JD031672. https://doi.org/10.1029/2019JD031672

Dirmeyer, P. A., Balsamo, G., Blyth, E. M., Morrison, R., & Cooper, H. M. (2021). Land-atmosphere interactions exacerbated the drought and heatwave over northern Europe during summer 2018. *AGU Advances, 2*(2), e2020AV000283. https://doi.org/10.1029/2020AV000283

Duan, Q., Schaake, J., Andréassian, V., Franks, S., Goteti, G., Gupta, H. V., et al. (2006). Model Parameter Estimation Experiment (MOPEX): An overview of science strategy and major results from the second and third workshops. *Journal of Hydrology, 320*(1), 3-17. https://doi.org/10.1016/j.jhydrol.2005.07.031

Gorelick, N., Hancher, M., Dixon, M., Ilyushchenko, S., Thau, D., & Moore, R. (2017). Google Earth Engine: Planetary-scale geospatial analysis for everyone. *Remote Sensing of Environment, 202*, 18-27. https://doi.org/10.1016/j.rse.2017.06.031

Greve, P., Orlowsky, B., Mueller, B., Sheffield, J., Reichstein, M., & Seneviratne, S. I. (2014). Global assessment of trends in wetting and drying over land. *Nature Geoscience, 7*(10), 716-721. https://doi.org/10.1038/ngeo2247

Greve, P., Roderick, M. L., Ukkola, A. M., & Wada, Y. (2019). The aridity Index under global warming. *Environmental Research Letters, 14*(12), 124006. https://doi.org/10.1088/1748-9326/ab5046

Hersbach, H., Bell, B., Berrisford, P., Hirahara, S., Horányi, A., Muñoz-Sabater, J., et al. (2020). The ERA5 global reanalysis. *Quarterly Journal of the Royal Meteorological Society, 146*(730), 1999-2049. https://doi.org/10.1002/qj.3803

Huang, J., Yu, H., Guan, X., Wang, G., & Guo, R. (2016). Accelerated dryland expansion under climate change. *Nature Climate Change, 6*(2), 166-171. https://doi.org/10.1038/nclimate2837

Huang, Y., Jin, Y., Schwartz, M. W., & Thorne, J. H. (2020). Intensified burn severity in California's northern coastal mountains by drier climatic condition. *Environmental Research Letters, 15*(10), 104033. https://doi.org/10.1088/1748-9326/aba6af

Keenan, T. F., Luo, X., Zhang, Y., & Zhou, S. (2020). Ecosystem aridity and atmospheric CO_2. *science, 368*(6488), 251-252. https://doi.org/10.1126/science.abb5449

Kim, Y., Garcia, M., Morillas, L., Weber, U., Black, T. A., & Johnson, M. S. (2021). Relative humidity gradients as a key constraint on terrestrial water and energy fluxes. *Hydrol. Earth Syst. Sci., 25*(9), 5175-5191. https://doi.org/10.5194/hess-25-5175-2021

Knauer, J., El-Madany, T. S., Zaehle, S., & Migliavacca, M. (2018). Bigleaf—An R package for the calculation of physical and physiological ecosystem properties from eddy covariance data. *PLOS ONE, 13*(8), e0201114. https://doi.org/10.1371/journal.pone.0201114

Liu, Z., Han, J., & Yang, H. (2022). Assessing the ability of potential evaporation models to capture the sensitivity to temperature. *Agricultural and forest meteorology, 317*, 108886. https://doi.org/10.1016/j.agrformet.2022.108886

Maes, W. H., Gentine, P., Verhoest, N. E. C., & Miralles, D. G. (2019). Potential evaporation at eddy-covariance sites across the globe. *Hydrol. Earth Syst. Sci., 23*(2), 925-948. https://doi.org/10.5194/hess-23-925-2019

Marvel, K., Cook, B. I., Bonfils, C. J. W., Durack, P. J., Smerdon, J. E., & Williams, A. P. (2019). Twentieth-century hydroclimate changes consistent with human influence. *Nature, 569*(7754), 59-65. https://doi.org/10.1038/s41586-019-1149-8

McColl, K. A., Salvucci, G. D., & Gentine, P. (2019). Surface flux equilibrium theory explains an empirical estimate of water-limited daily evapotranspiration. *Journal of Advances in Modeling Earth Systems, 11*(7), 2036-2049. https://doi.org/10.1029/2019ms001685

McEvoy, D. J., Pierce, D. W., Kalansky, J. F., Cayan, D. R., & Abatzoglou, J. T. (2020). Projected Changes in Reference Evapotranspiration in California and Nevada: Implications for Drought and Wildland Fire Danger. *Earth's Future, 8*(11), e2020EF001736. https://doi.org/10.1029/2020EF001736

McNally, A., Arsenault, K., Kumar, S., Shukla, S., Peterson, P., Wang, S., et al. (2017). A land data assimilation system for sub-Saharan Africa food and water security applications. *Scientific Data, 4*(1), 170012. https://doi.org/10.1038/sdata.2017.12

Milly, P. C. D., & Dunne, K. A. (2016). Potential evapotranspiration and continental drying. *Nature Climate Change, 6*(10), 946-949. https://doi.org/10.1038/nclimate3046

Milly, P. C. D., & Dunne, K. A. (2017). A hydrologic drying bias in water-resource impact analyses of anthropogenic climate change. *JAWRA Journal of the American Water Resources Association, 53*(4), 822-838. https://doi.org/10.1111/1752-1688.12538

Milly, P. C. D., & Dunne, K. A. (2020). Colorado River flow dwindles as warming-driven loss of reflective snow energizes evaporation. *science, 367*(6483), 1252-1255. https://doi.org/10.1126/science.aay9187

Mladenova, I. E., Bolten, J. D., Crow, W., Sazib, N., & Reynolds, C. (2020). Agricultural Drought Monitoring via the Assimilation of SMAP Soil Moisture Retrievals Into a Global Soil Water Balance Model. *Frontiers in Big Data, 3*(10). Original Research. https://doi.org/10.3389/fdata.2020.00010

Monteith, J. L. (1965). *Evaporation and environment.* Paper presented at the Symposia of the society for experimental biology.

Overpeck, J. T., & Udall, B. (2020). Climate change and the aridification of North America. *Proceedings of the National Academy of Sciences, 117*(22), 11856-11858. https://doi.org/10.1073/pnas.2006323117

Pastorello, G., Trotta, C., Canfora, E., Chu, H., Christianson, D., Cheah, Y.-W., et al. (2020). The FLUXNET2015 dataset and the ONEFlux processing pipeline for eddy covariance data. *Scientific Data, 7*(1), 225. https://doi.org/10.1038/s41597-020-0534-3

Piemontese, L., Fetzer, I., Rockström, J., & Jaramillo, F. (2019). Future Hydroclimatic Impacts on Africa: Beyond the Paris Agreement. *Earth's Future, 7*(7), 748-761. https://doi.org/10.1029/2019EF001169

Priestley, C. H. B., & Taylor, R. J. (1972). On the assessment of surface heat flux and evaporation using large-scale parameters. *Monthly Weather Review, 100*(2), 81-92. https://doi.org/10.1175/1520-0493(1972)100<0081:otaosh>2.3.co;2

R CORE TEAM. (2018). R: A language and environment for statistical computing. *R Foundation for Statistical Computing, Viena, Austria, Vienna, Austria*.

Rigden, A. J., & Salvucci, G. D. (2017). Stomatal response to humidity and CO_2 implicated in recent decline in US evaporation. *Global Change Biology, 23*(3), 1140-1151. https://doi.org/10.1111/gcb.13439

Roderick, M. L., Greve, P., & Farquhar, G. D. (2015). On the assessment of aridity with changes in atmospheric CO_2. *Water Resources Research, 51*(7), 5450-5463. https://doi.org/10.1002/2015WR017031

Salvucci, G. D., & Gentine, P. (2013). Emergent relation between surface vapor conductance and relative humidity profiles yields evaporation rates from weather data. *Proceedings of the National Academy of Sciences, 110*(16), 6287-6291. https://doi.org/10.1073/pnas.1215844110

Scheff, J., & Frierson, D. M. W. (2014). Scaling Potential Evapotranspiration with Greenhouse Warming. *Journal of Climate, 27*(4), 1539-1558. https://doi.org/10.1175/jcli-d-13-00233.1

Sheffield, J., Wood, E. F., & Roderick, M. L. (2012). Little change in global drought over the past 60 years. *Nature, 491*(7424), 435-438. https://doi.org/10.1038/nature11575

Sherwood, S., & Fu, Q. (2014). A drier future? *science, 343*(6172), 737-739. https://doi.org/10.1126/science.1247620

Shi, H., Tian, H., Lange, S., Yang, J., Pan, S., Fu, B., & Reyer, C. P. O. (2021). Terrestrial biodiversity threatened by increasing global aridity velocity under high-level warming. *Proceedings of the National Academy of Sciences, 118*(36), e2015552118. https://doi.org/10.1073/pnas.2015552118

Su, B., Huang, J., Fischer, T., Wang, Y., Kundzewicz, Z. W., Zhai, J., et al. (2018). Drought losses in China might double between the 1.5 °C and 2.0 °C warming. *Proceedings of the National Academy of Sciences, 115*(42), 10600-10605. https://doi.org/10.1073/pnas.1802129115

Swann, A. L. S., Hoffman, F. M., Koven, C. D., & Randerson, J. T. (2016). Plant responses to increasing CO_2 reduce estimates of climate impacts on drought severity. *Proceedings of the National Academy of Sciences, 113*(36), 10019-10024. https://doi.org/10.1073/pnas.1604581113

Taylor, K. E., Stouffer, R. J., & Meehl, G. A. (2012). An overview of CMIP5 and the experiment design. *Bulletin of the American Meteorological Society, 93*(4), 485-498. https://doi.org/10.1175/bams-d-11-00094.1

Tomas-Burguera, M., Vicente-Serrano, S. M., Peña-Angulo, D., Domínguez-Castro, F., Noguera, I., & El Kenawy, A. (2020). Global Characterization of the Varying Responses of the Standardized Precipitation Evapotranspiration Index to Atmospheric Evaporative Demand. *Journal of Geophysical Research: Atmospheres, 125*(17), e2020JD033017. https://doi.org/10.1029/2020JD033017

Trenberth, K. E., Dai, A., van der Schrier, G., Jones, P. D., Barichivich, J., Briffa, K. R., & Sheffield, J. (2013). Global warming and changes in drought. *Nature Climate Change, 4*, 17. Perspective. https://doi.org/10.1038/nclimate2067

Tu, Z., Yang, Y., & Roderick, M. L. (2022). Testing a maximum evaporation theory over saturated land: implications for potential evaporation estimation. *Hydrol. Earth Syst. Sci., 26*(7), 1745-1754. https://doi.org/10.5194/hess-26-1745-2022

Vicente-Serrano, S. M., McVicar, T. R., Miralles, D. G., Yang, Y., & Tomas-Burguera, M. (2020). Unraveling the influence of atmospheric evaporative demand on drought and its response to climate change. *WIREs Climate Change, 11*(2), e632. https://doi.org/10.1002/wcc.632

Wang, W., Lee, X., Xiao, W., Liu, S., Schultz, N., Wang, Y., et al. (2018). Global lake evaporation accelerated by changes in surface energy allocation in a warmer climate. *Nature Geoscience, 11*(6), 410-414. https://doi.org/10.1038/s41561-018-0114-8

Yang, Y., Roderick, M. L., Zhang, S., McVicar, T. R., & Donohue, R. J. (2019). Hydrologic implications of vegetation response to elevated CO_2 in climate projections. *Nature Climate Change, 9*(1), 44-48. https://doi.org/10.1038/s41558-018-0361-0

Yang, Y., Zhang, S., Roderick, M. L., McVicar, T. R., Yang, D., Liu, W., & Li, X. (2020). Comparing Palmer Drought Severity Index drought assessments using the traditional offline approach with direct climate model outputs. *Hydrol. Earth Syst. Sci., 24*(6), 2921-2930. https://doi.org/10.5194/hess-24-2921-2020